Electrostatic Stability of a Large Collection of Charged Anisotropic Nanoparticles: A Monte Carlo Study Exploiting a Hierarchical Approach

A. Delville*

CRMD, CNRS, 1B rue de la Férollerie, 45071 Orléans Cedex 02, France

Received: March 1, 2006; In Final Form: May 3, 2006

We have performed Monte Carlo simulations of the self-organization of large collections of charged disks of various electric charges to probe the influence of electrostatic coupling on the structure and the mechanical stability of aqueous dispersions of charged anisotropic nanoparticles in the presence of salt. A hierarchical approach of the long-range Coulombic potential was used to perform such Monte Carlo simulations of a large number of charged species. By analyzing the influence of the net electric charge of the disks on their self-organization, we detected a negative contribution to the mean force potential resulting from their electrostatic coupling. In addition, it has been shown that the same electrostatic coupling restricts the spatial extend of locally ordered microdomains within dilute dispersions of charged anisotropic colloids.

I. Introduction

Throughout many decades, the mechanical stability of aqueous dispersions of charged colloids neutralized by monovalent counterions is well described on the basis of the Derjaguin, Landau, Verwey, and Overbeek (DLVO) theory.[1,2] The correlation forces are then negligible,[3−5] and the long-range repulsion between the charged colloids results simply from the overlap[1−2,6−10] of their clouds of condensed counterions whose thickness is modulated by the salt concentration.[9,10] In that framework, anisotropic colloids are recently the subject of various studies because of some intriguing mechanical behavior[11,12] detected in the presence of salt. In addition to the long-range electrostatic coupling, various couplings such as finite size effects,[13−14] hydrodynamic flow,[15] or magnetic[16,17] interactions have been shown to favor the formation of nematic phases within such dispersions of anisotropic colloids. Furthermore, recent analysis of light scattering[18] and SAXS[18,19] experiments suggests the existence of a microsegregation of the clay platelets within the dispersion and a short-ranged attraction between the charged clay particles. The origin of this attraction is not clear since theoretical treatments of the electrostatic coupling between a pair of such colloids[20−23] always exhibits a net repulsion between the charged disks. The purpose of this study is to perform Monte Carlo simulations to quantify the influence of the electrostatic coupling within a large collection of charged disks. In the framework of the primitive model,[24] recent Monte Carlo simulations have already shown a significant decrease of the net electrostatic repulsion between three charged spheres[25,26] or three charged parallel cylinders[27] induced by many-body interactions. But, in the case of charged disks, previous treatments have only considered the distribution of the counterions around a single[23] or a pair[20−22] of charged disks to evaluate their net electrostatic repulsion. Large collections of charged disks were previously treated in an approximate manner, either by describing the net interaction between the charged disk, by using an effective Yukawa potential,[28,29] or by focusing on the electrostatic quadrupole[30] originating from the net electric charges of the disk in addition to its cloud of condensed monovalent counterions.

In that context, we have considered a large collection of rigid disks dispersed in dilute regime in equilibrium with a salt reservoir. To probe the influence of electrostatic coupling, the net electric charge of the disks varies between 25 and 400 e. This maximum electric charge of disks correspond to half of the nominal charge of Laponite synthetic clays widely used for experimental studies.[18−19,39,42−48] However, because of the large number of ions (more than 10^5) involved in these numerical simulations, it is not possible with the current available computers to treat exactly the electrostatic coupling between all the charged entities (ions plus charged disks). We have thus developed a hierarchical approximation[31,32] of the electrostatic coupling based on a multipolar expansion of the Coulombic potential at large separations.

Furthermore, due to the strong condensation of the monovalent counterions at the surface of the charged disks, it is necessary to perform the Monte Carlo sampling of the configurations of the charged disks by displacing each charged disk with its cloud of condensed counterions.[32] A Rosenbluth sampling[33] procedure is used to thermalize the ionic configurations during these global displacements of the charged disks and their condensed counterions. The acceptation ratio corresponding to the disk displacement is further improved by using positional[34] and orientational[35] statistical biases.

These numerical simulations clearly exhibit an enhancement of the center-to-center radial distribution function describing the organization of the charged disks bearing half of the nominal electric charges of the synthetic Laponite clays. Since no dispersion forces are included in these simulations, the electrostatic origin of this organization can be clearly identified. Two phenomena may be responsible for the detected enhancement of the radial distribution function: either a short-ranged attraction between the charged disks resulting from many-body interactions or a long-range repulsion responsible for the solidification of the dispersion. We are not able to settle this question because of the large numerical uncertainties in the derivation of the swelling pressure of the dispersion.

* E-mail: delville@cnrs-orleans.fr.

10.1021/jp0612883 CCC: $33.50
Published on Web 05/27/2006

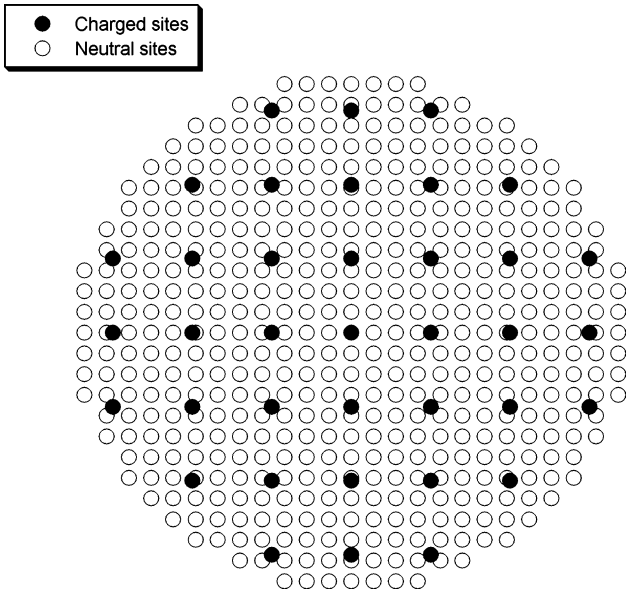

Figure 1. Top view of the network of 37 charged sites located in the equatorial plane of the disk and one surface network of 489 neutral sites used to check for volume exclusion between the disks.

II. Methods

A. Modeling the Clay Dispersion. The electrostatic coupling between the rigid disks (thickness 10 Å, diameter 300 Å)[36] and the ions (diameter 4.5 Å) is described in the framework of the primitive model[24] by using the dielectric constant of bulk water. The size of the ions and rigid disks are selected to mimic hydrated sodium cations and Laponite synthetic clays, respectively. An amount of 343 rigid disks were dispersed in a large simulation cell (width 2800 Å) describing a dilute clay dispersion (~3% W/W). Simulations are performed at various net electric charges of the disks (25, 50, 100, 200, and 400 e) to gradually probe the influence of the electrostatic coupling on the structure and the stability of the clay dispersion. The largest electric charge corresponds to half of the nominal charge of the synthetic Laponite clay. Whatever the net electric charge of the disks, 37 equivalent charged sites are uniformly distributed on a squared network located in the equatorial plane of the disks (see Figure 1). The electric charge of each interacting site is thus obtained by dividing the net electric charge of the disk by the total number of sites per disk (i.e., 37). The location of the electric charges within the equatorial plane of the disks is selected to describe the location of the substitution sites of the Laponite clay which are responsible for the net electric charge of this colloid. Two supplementary networks of 489 neutral sites are uniformly spread on the basal surfaces of the disks (see Figure 1) and used to check for the excluded volume interaction between the disks. Grand canonical Monte Carlo simulations are performed to mimic the ionic exchange[5] between the clay dispersion and a reservoir of fixed ionic strength ($I = 5\ 10^{-3}$ M). The initial position of charged disks corresponds to a perfect crystal with a cubic network, while the orientations of disks are totally random. The melting of this initial colloidal crystal is a good index of its thermalization. The initial configuration of the sodium counterions is generated by a Rosenbluth sampling,[33] generating 6×10^6 trial positions within the whole simulation cell.

B. Hierarchical Approximation. Because of the large number of labile ions, it is necessary to approximate the Coulombic potential at large distances by a multipolar expansion. For that purpose, the whole simulation cell is divided within 343 smaller cubes[32] (width 400 Å). In the framework of that hierarchical approximation of the Coulomb potential,[31−32] the whole simulation cell is divided into three domains (see Figure 2): the central cell (noted CC), its 26 first neighboring cells (noted NC), and the 361 remaining remote cells (noted RC). The electric charges pertaining to all ions and charged disks located within each remote cell are replaced by 18 variable charges located at fixed sites inside the remote cell: 6 sites are localized at the center of each face of the remote cell and 12 sites are at the center of each side. The electric charges located on each facing face are opposite to each other and selected to reproduce the corresponding component of the dipolar moment of the electric charges located within the remote cell. By contrast, the electric charges located on the two side sites resulting from a central symmetry through the center of the remote cell are set equal to each other and selected to reproduce the total electric charge and the five quadrupolar components of the charge distribution within the remote cell. Elementary algebra is used to determine the unique set of nine fixed charges from the nine independent multipolar components of electric charges located within the remote cell.

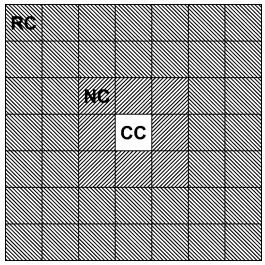

Figure 2. 2D illustration of the central cell (CC) with its neighboring (NC) and remote (RC) cells used for the hierarchical approximation of the electrostatic potential (see text).

The electrostatic energy of an ion (labeled i) located in the central cell (CC) results from three contributions. The first contribution results from the exact Coulombic potential generated by all of the ions (labeled j) and charged disks (labeled m) located in the same CC (eq 1a). The second contribution (eq 1b) results from the exact Coulombic potential generated by ions (labeled k) and charged disks (labeled n) located in 26 neighboring cells (labeled a). Note that labels α and β in eqs 1a and 1b describe the 37 charged sites of the disks (labeled, respectively, m and n). Finally, eq 1c describes the electrostatic coupling of the ion labeled i with each of 18 variable sites (labeled o) located within 316 remote cells (labeled b).

$$E_i = \frac{q_i}{4\pi\epsilon_0\epsilon_r}\left[\sum_{\substack{j\in CC\\ j\neq i}}\frac{q_j}{r_{ij}} + \sum_{m\in CC}\sum_{\substack{\alpha=1\\ \alpha\in m}}^{37}\frac{q_\alpha}{r_{i\alpha}}\right] \quad (1a)$$

$$+ \frac{q_i}{4\pi\epsilon_0\epsilon_r}\left[\sum_{\substack{a=1\\ a\in NC}}^{26}\left\{\sum_{k\in a}\frac{q_k}{r_{ik}} + \sum_{n\in a}\sum_{\substack{\beta=1\\ \beta\in n}}^{37}\frac{q_\beta}{r_{i\beta}}\right\}\right] \quad (1b)$$

$$+ \frac{q_i}{4\pi\epsilon_0\epsilon_r}\left[\sum_{\substack{b=1\\ b\in RC}}^{316}\sum_{\substack{o=1\\ o\in b}}^{18}\frac{q_o}{r_{io}}\right] \quad (1c)$$

In the same manner, the electrostatic energy of a charged disk (labeled p) results from the electrostatic coupling of its 37 charged sites (labeled γ) with electric charges located within the same CC (eq 2a), the 26 neighboring cells (eq 2b), and the 316 remote cells (eq 2c).

$$E_p = \frac{1}{4\pi\epsilon_0\epsilon_r}\left[\sum_{\substack{\gamma=1\\ \gamma\in p}}^{37} q_\gamma \left\{\sum_{j\in CC} \frac{q_j}{r_{\gamma j}} + \sum_{\substack{m\in CC\\ m\neq p}} \sum_{\substack{\alpha=1\\ \alpha\in m}}^{37} \frac{q_\alpha}{r_{\gamma\alpha}}\right\}\right] \quad (2a)$$

$$+ \frac{1}{4\pi\epsilon_0\epsilon_r}\left[\sum_{\substack{\gamma=1\\ \gamma\in p}}^{37} q_\gamma \sum_{\substack{a=1\\ a\in NC}}^{26} \left\{\sum_{k\in a} \frac{q_k}{r_{\gamma k}} + \sum_{n\in a} \sum_{\substack{\beta=1\\ \beta\in n}}^{37} \frac{q_\beta}{r_{\gamma\beta}}\right\}\right] \quad (2b)$$

$$+ \frac{1}{4\pi\epsilon_0\epsilon_r}\left[\sum_{\substack{\gamma=1\\ \gamma\in p}}^{37} q_\gamma \sum_{\substack{b=1\\ b\in RC}}^{316} \sum_{\substack{o=1\\ o\in b}}^{18} \frac{q_o}{r_{\gamma o}}\right] \quad (2c)$$

Of course, periodic boundary conditions are used to evaluate this approximate electrostatic potential. Because of the ionic strength of the reservoir ($I = 5 \times 10^{-3}$ M), the range of the effective electrostatic repulsion[9] between charged disks does not exceed 42 Å, a priori validating our approximation since we explicitly consider the exact Coulombic potential at separations larger by 1 order of magnitude.

Within the same approach, the total pressure of the dispersion has been evaluated by calculating the internal virial[37] resulting from the internal forces ($\mathbf{F}_i^{int}$) acting on ions and charged disks

$$P = \frac{(N_i + N_d)kT}{V} + \frac{1}{3V}\left\langle \sum_i^{N_i+N_d} \vec{R}_i * \vec{F}_i^{\,int} \right\rangle \quad (3)$$

The first term of eq 3 describes the ideal contribution to the total pressure of the dispersion, and the second term describes the contribution from the interparticle interactions. Since these rigid disks contain many electrostatic sites, their center of mass ($\mathbf{R}_i$) does not necessarily coincide with their interacting sites ($\mathbf{r}_\alpha$). As a consequence, the contribution from internal forces becomes[38]

$$\sum_i^{N_i+N_d} \vec{R}_i * \vec{F}_i^{\,int} = -\frac{1}{2} \sum_i^{N_i+N_d} \sum_{\alpha\in i} \sum_{j\neq i}^{N_i+N_d} \sum_{\beta\in j} \frac{\vec{R}_{ij} * \vec{r}_{\alpha\beta}}{r_{\alpha\beta}} \frac{\mathrm{d}u_{\alpha\beta}}{\mathrm{d}r_{\alpha\beta}} \quad (4)$$

where N_i and N_d are, respectively, the total number of ions and disks, $\mathbf{R}_{ij}$ is the relative position of the center of mass of a pair of ions and/or disks, $\mathbf{r}_{\alpha\beta}$ is the relative position of two interacting sites α and β located on particles i and j, respectively, and $u_{\alpha\beta}$ is the corresponding pair potential. It is obvious that the single interacting site of the ions coincides with their center of mass. The contribution from the ion/disk contact forces is evaluated in the same manner by extrapolating the sodium concentration profiles to contact with the basal and lateral surfaces[38] of the charged disks (see Figures 3)

$$P_{\text{ion-disk}}^{\text{contact}} = \frac{kT}{3V} \sum_{i=1}^{N_d} \int_{S_i} (c_{Na}(S) + c_{Cl}(S))\vec{n}_S * \vec{r}_{iS}\, \mathrm{d}S \quad (5)$$

where S_i is the surface of the disk labeled i, $\mathbf{n}_S$ is the outer normal to its surface, $c_{Na}(S)$ and $c_{Cl}(S)$ are the cationic and anionic densities extrapolated at contact with the disk surface, and $\mathbf{r}_{iS}$ is the vector joining the center of mass of the disk labeled i and the envelope of the contact points of different ions at the disk surface. The contribution from the ion/ion contact force is finally evaluated by extrapolating the ion/ion radial distribution function[37] to contact

$$P_{\text{ions}}^{\text{contact}} = \frac{2\pi kT}{3} \sum_i^{N_i} {\rho_i}^0 \sum_j^{N_j} {\rho_j}^0 {\sigma_{ij}}^3 g_{ij}(\sigma_{ij}) \quad (6)$$

where N_i is the total number of ions (labeled i) with an average density ρ_i^0, σ_{ij} is the ionic diameter (4.5 Å), and g_{ij} is the ion/ion radial distribution function.

C. Statistical Biases. Positional[34] and orientational[35] statistical biases are used to improve the acceptance ratio during the displacement of rigid disks. For that purpose, a disk is selected randomly within its initial small cube (400 Å width), and a final small cube is selected randomly with its 26 first neighboring cubes disjoined[32] from the initial cube and its own 26 first neighbors. An amount of 218 such disjoined cubes are available in the simulation cell. Then a cavity sampling[34] is performed by generating randomly 100 trial positions within the final cube. Among these 100 trial positions, we only consider those located at more than 30 Å from the center of mass of other disks. Let us assume N_{pos} is the total number of such available new positions. The ratio (facto1 = N_{pos}/100) defines the probability of generating a new position of the center of mass of the charged disk in the final cube. To satisfy the detailed balance condition,[34] the corresponding probability (facto2) is also evaluated for the initial disk in its own initial cube.

Second, we select randomly one of these N_{pos} trial positions and generate randomly 30 different orientations[35] of the rigid disk centered on this selected position. Among these 30 new orientations, only those orientations (noted N_{ang}), for which the new rigid disk does not overlap other disks, are recorded, thus defining the orientational probability (facto3 = N_{ang}/30). As before, the same orientational sampling[35] is performed at the initial position of the disk, leading to the orientational probability (facto4) of generating the initial orientation of the rigid disk by the same procedure.

Next, the sets of ions located within the initial and final cubes are swapped.[32] For that purpose, all ions (noted Nmouv1) located at less than 250 Å from the center of mass of the initial disk in the initial cube and its 26 first neighbors are selected and will move with the initial selected disk. During that global motion, all ions (noted Nmouv2) located in the final cube and its first neighbors at a separation smaller than 250 Å from the final position of the disk are also selected and put back in the empty cavity from the initial cube. Finally, Rosenbluth samplings[33] are performed to optimize the location of ions moved in the final and initial cavities. Thanks to the complete separation between the initial and the final cubes, both procedures may be performed independently. As for the positional[34] and orientational[35] biases, the generating probability are evaluated during the Rosenbluth samplings[33] to satisfy the microreversibility condition. More details on this Rosenbluth sampling are given in a previous article.[32] This global sampling procedure raises the acceptation ratio for the trial displacement of a charged disk up to 50% at the lowest electric charges and 10% at the highest.

After each trial displacement of a charged disk and its condensed counterions, we perform 10 000 elementary grand canonical Monte Carlo steps concerning the ions located within the initial and final cubes to equilibrate the salt concentration[5] of the colloidal dispersion with that of a reservoir at fixed ionic strength ($I = 5 \times 10^{-3}$ M).

III. Result and Discussion

Figure 3 displays the ionic concentration profiles near to the basal (parts a and b of Figure 3) and the lateral (parts c and d of Figure 3) surfaces of the disks. Even at the weakest surface charge density, the local concentration of the counterions in

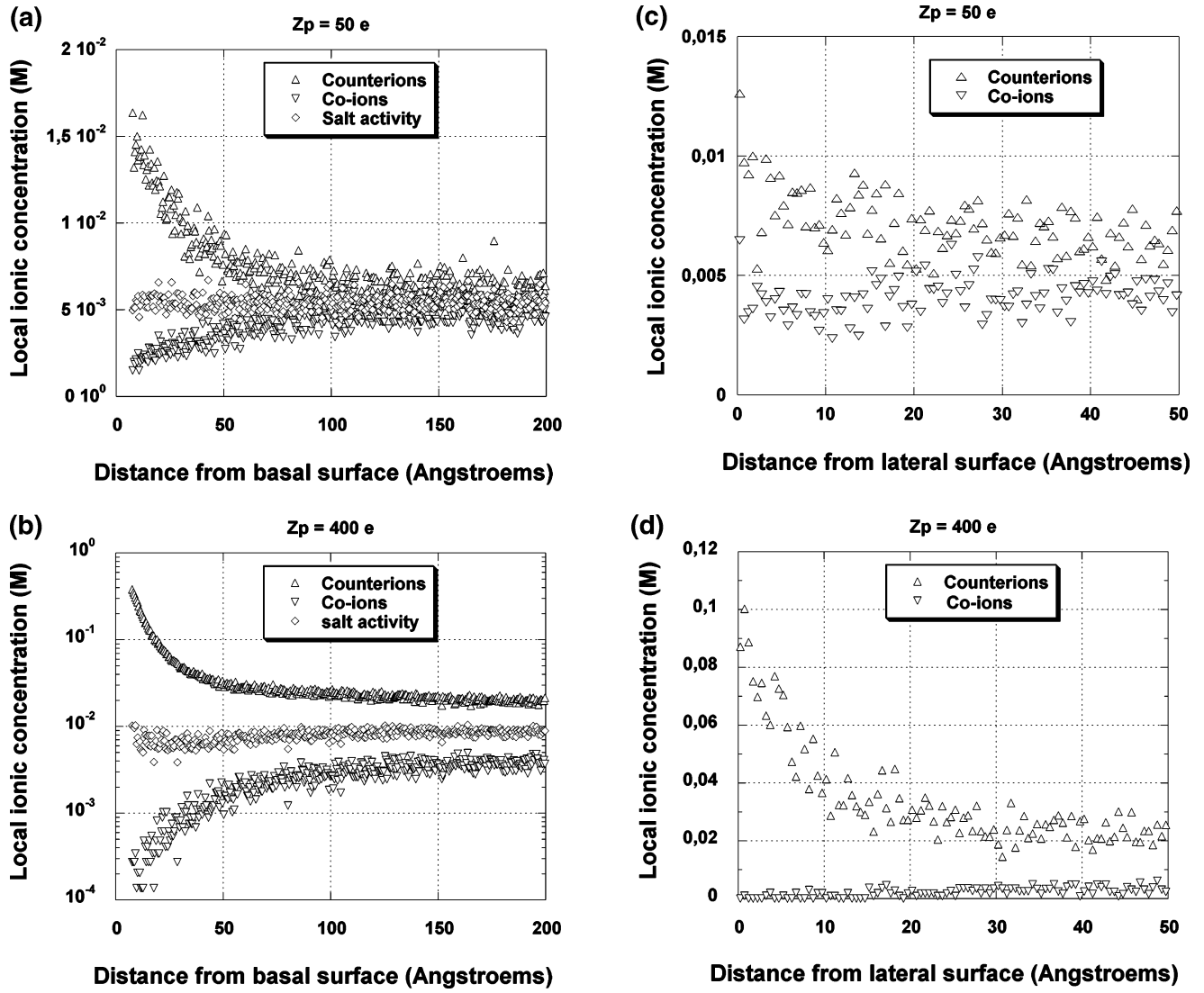

Figure 3. Concentration profiles of the counterions and co-ions illustrating the ionic condensation on the basal (parts a and b) and lateral (parts c and d) surfaces of the charged disks obtained with 50 (parts a and c) and 400 (parts b and d) electrons per disk. The salt activity is evaluated from the square root of the product of the local ionic concentrations (see text).

contact with the basal surface of the charged disk is three times larger than the bulk concentration (see Figure 3a). Of course, this accumulation of counterions is weak compared with the phenomenon of ionic condensation. This counterion accumulation increases gradually as a function of the strength of the electrostatic coupling, leading to a strong ionic condensation at the highest electric charge (see Figure 3b). By contrast, the ionic concentration profile exhibits a reduced accumulation of the counterions on the lateral surface of weakly charged disks (see Figure 3c) while a noticeable condensation of the sodium counterions is detected on the lateral surface of the disks at the highest electric charge (see Figure 3d). This figure clearly exhibits the propagation of the electrostatic potential in the lateral domain surrounding the charged disk. It also illustrates the efficiency of such clay particles to act as a diffusional barrier even within dilute dispersions by trapping a large number of counterions in their vicinity, thus slowing down their mobility.[39]

As a consequence of the chemical exchange of the dissociated salt molecules between the dispersion and its reservoir, the square root of the product of the local cationic and ionic densities matches the salt concentration of the reservoir.[10] This result, which is at the basis of the Donnan salt exclusion phenomenon,[9−10] is also a powerful check of the validity of our GCMC sampling. Figure 4 displays the influence of the net electric charge of the disk on the strength of this Donnan exclusion phenomenon. Even at large separation between charged disks (at 3% W/W, the average separation between the disks is 400 Å), the real salt concentration within the dispersion is lowered by 13% compared with the salt concentration in the reservoir ($c_{salt}^{reservoir} = 5 \times 10^{-3}$ M). To check the validity of the Poisson−Boltzmann[23,40] (PB) approximation, Figure 4 also displays the Donnan exclusion factor evaluated within the PB formalism by using the cell model.[10] For that purpose, two parallel infinite planes are facing each other with a uniform surface electric charge (σ). The period (P) of this cell (i.e., the separation between the charged planes) is fixed to reproduce the average surface/volume ratio of the dispersion of charged disks

$$\left(\frac{S}{V}\right)_{PB} = \frac{2}{P} = \left(\frac{S}{V}\right)_{GCMC} = \frac{2\pi 150^2}{400^3} = 2.2 \times 10^{-3}\ \text{Å}^{-1} \quad (7a)$$

leading to a period of 905 Å. Since the product of the Debye screening factor (κ) by the period of the Wigner cell (P) is larger than unity ($\kappa P = 22.6$), the Donnan exclusion factor may be

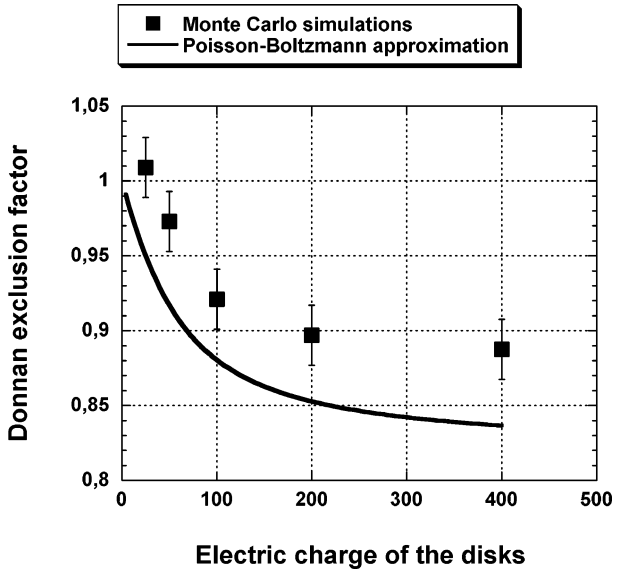

Figure 4. Illustration of the Donnan exclusion phenomenon evaluated from the ratio between the average salt concentration in the dispersion and the salt concentration of the reservoir (5×10^{-3} M). The black squares are GCMC results, and the continuous curve is calculated from the Poisson−Boltzmann formalism (see text).

evaluated in the PB framework[10] by the simple relationship

$$\frac{c_{\text{salt}}^{\text{dispersion}}}{c_{\text{salt}}^{\text{reservoir}}} = 1 - \frac{2\gamma}{1+\gamma}\frac{4}{\kappa P} \tag{7b}$$

with

$$\gamma = \sqrt{1 + \left(\frac{1}{E}\right)^2} - \frac{1}{E} \tag{7c}$$

where $E = (2\pi L_B \sigma)/(\kappa e)$, σ is the electric surface charge density of the disk, κ is the Debye screening constant (2.38×10^{-2} Å^{-1}), and L_B is the Bjerrum length ($L_B = e^2/[4\pi\epsilon_0\epsilon_r kT] = 7.2$ Å for water at room temperature). As shown in Figure 4, the PB approximation slightly overestimates the Donnan exclusion phenomenon probably because of the cell model, where infinite parallel charged interfaces are used, overestimates the overlap of the diffuse layers surrounding the charged disks. On the basis of this semiquantitative agreement, one may reasonably expect that a numerical solution of the PB equation will perfectly reproduce the results of our GCMC simulations by explicitly taking into account the finite size of the charged disks[23,40] and their spatial organization.

Figure 5a displays the total electrostatic energy of the dispersion together with its different contributions as a function of net electric charge of the disks. As a consequence of the counterion condensation, the ion/ion and colloid/colloid electrostatic repulsions are strongly compensated by the counterion/colloid attraction, leading to a net electrostatic attraction between the charged disks neutralized by monovalent counterions. This result is generally observed for charged particles of any shape,[27] whatever the valency[5,20−22] of their counterions. Figure 5a also exhibits a very weak contribution form the long-range multipolar expansion,[31−32] ensuring the convergence of our hierarchical approximation (see IIB above). In the absence of any saturation, it is expected that the total electrostatic energy increases as the square of the net electric charges of the disks (cf. Figure 5b). As a consequence, enough empty space is available at the surface of charged disks for the occurrence of ionic condensation, even at the highest surface charge density of the colloids.

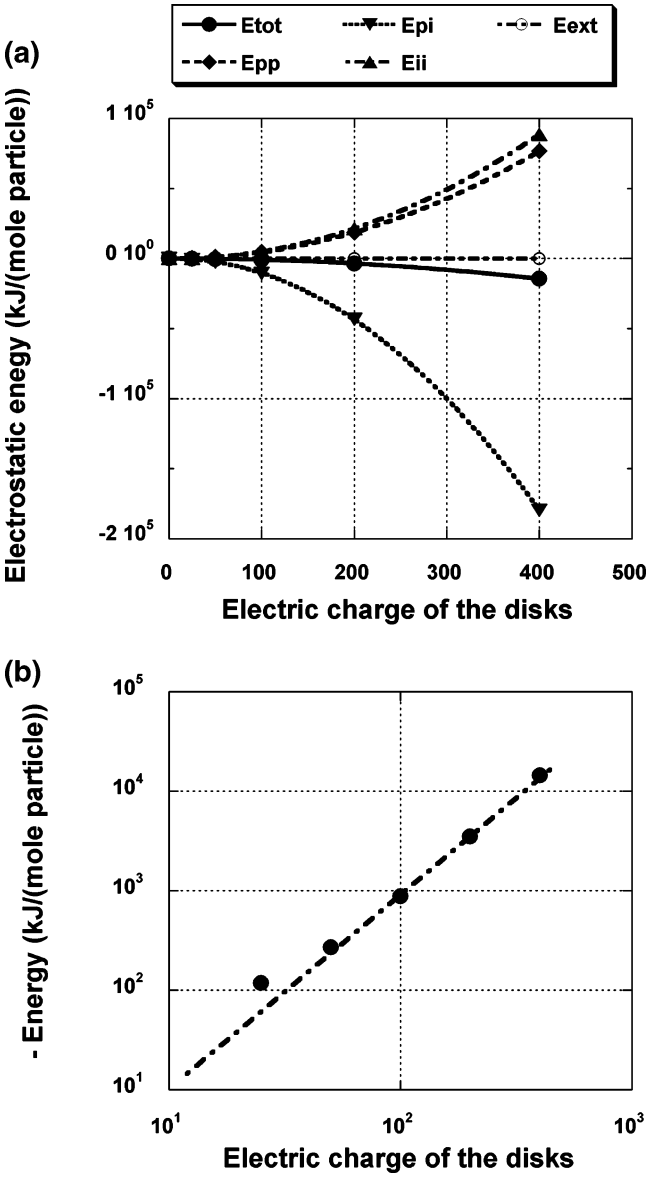

Figure 5. Variation of the total electrostatic energy (E_{tot}) with its different contributions as a function of the electric charge of the disks. The exact Coulombic contributions are E_{pp} (disk/disk), E_{pi} (disk/ion), and E_{ii} (ion/ion) while E_{ext} is the long-range contribution resulting from the multipolar approximation (see text). The size of the symbols corresponds to the numerical uncertainties. The log/log plot used in Figure 5b helps to better visualize the power law variation of the total electrostatic energy.

The influence of electrostatic coupling on the self-organization of the charged disks is obtained by comparing their local order parameters ($O(r)$) (see Figure 6) and their center-to-center radial distribution functions (see Figure 7) as a function of the nominal electric charge of the disks. The local order parameter is evaluated from the angle between the two normals characterizing the orientation of the central disk and those located at a distance (r)

$$O(r) = \left\langle \frac{3\cos^2\theta(r) - 1}{2} \right\rangle \tag{8}$$

The local order parameter is used to quantify the relative orientation of neighboring disks within the dispersion as a

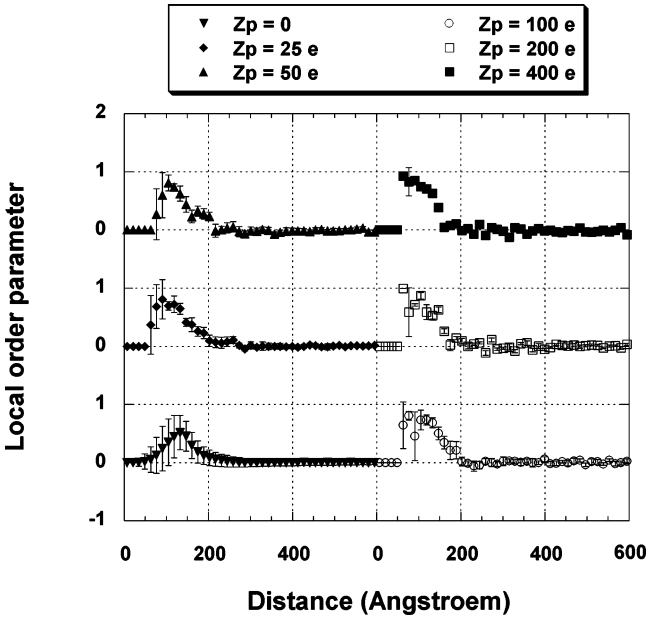

Figure 6. Local order parameter (see text) evaluated at different electric charge of the disks.

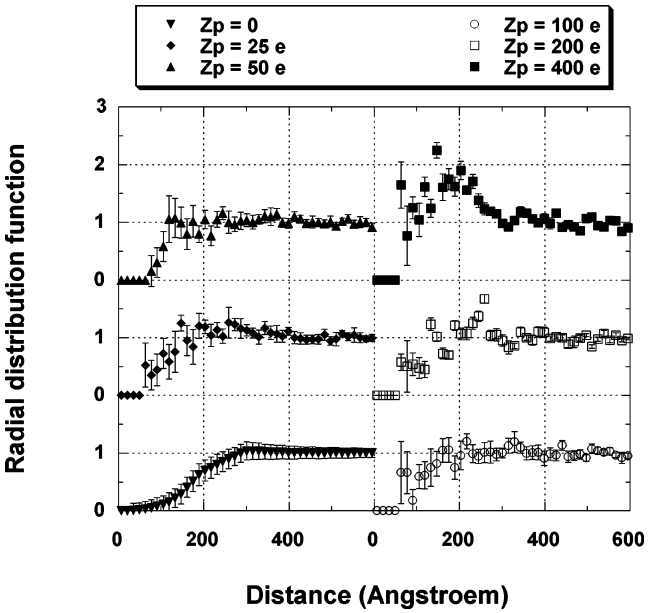

Figure 7. Variation of the disk/disk radial distribution function as a function of the electric charge of the disks.

function of their electric charge. This discussion is interesting since two antagonistic contributions monitor the organization of the clay dispersions: (1) first, the excluded volume interaction,[13−14,41] which optimizes the entropy of the dispersion by a parallel alignment of the disks; (2) second, the electrostatic coupling, which was shown recently to minimize the free energy of the dispersion by a relative perpendicular orientation[22] of neighboring charged disks.

As a consequence, the electrostatic coupling is expected to inhibit the occurrence of the isotrope/nematic phase transition within such dispersions of charged anisotropic colloids, in complete agreement with NMR spectroscopic measurements performed on diluted[39] and concentrated[44−48] clay dispersions. As shown in Figure 6, the parallel ordering of the disk dispersion in this dilute regime (∼3% W/W) remains only local (i.e., below 200 Å). Above that separation, the local order parameter is zero, corresponding to fully decorrelated orientation of charged disks,

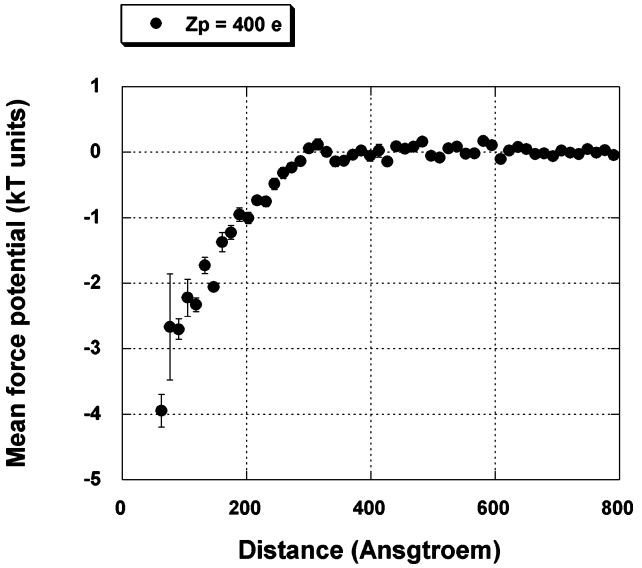

Figure 8. Electrostatic contribution to the mean force potential within the dispersion of the most charged disks (400 electrons) evaluated from the radial distribution functions (see text).

as shown by ^{23}Na NMR relaxometry measurements.[39] Finally, one also notes in Figure 6 a significant reduction of the spatial extend of the locally ordered microdomains whose maximum size reduce from 200 to 160 Å when the electric charge of the disks reaches 400 e. This result is important since the occurrence of some microstructure within the clay dispersion, corresponding to a relative perpendicular orientation of the neighboring colloids, is not only compatible with the minimization of the electrostatic contribution to the free energy of these charged anisotropic colloids[49] but also it may lead to some local locks responsible for the occurrence of the sol/gel transition[42,43] of the dispersion. Let us simply remember that a fully nematic phase does not exhibit any yield stress such as that reported by the rheological behavior of Laponite clay dispersions.[42]

As shown in Figure 7, the radial distribution function of disks does not vary too much when the electric charge of the disks increases from 25 to 200 e: the radial distribution function is almost equal to unity and no structure is detected at distances larger than 150 Å. Below that limit, the radial distribution functions (RDFs) slowly decrease to zero because of excluded volume effects. But, at an electric charge of 400 e per disk, the RDF largely exceeds 1 at separations varying between 100 and 250 Å while the average separation between the disk is 400 Å. Figure 8 further displays the electrostatic contribution to the mean force potential characterizing the dispersion of the disks bearing the highest nominal charge (i.e., 400 e) by dividing their RDF by the RDF evaluated for the disks bearing the weakest electric charge (i.e., 25 e). One may be tempted to identify the negative contribution to the mean force potential detected below 300 Å (cf. Figure 8) with the attractive pair potential obtained from an HNC inversion[18] of the small-angle X-ray and light scattering experiments performed on Laponite dispersions (see Figure 9 in ref 18). Such a behavior suggests the possible existence of an instability of the dispersion resulting from the electrostatic coupling which may be responsible for the flocculation of the Laponite dispersion in the presence of salt.[42−43] This analysis is probably justified in the case of spherical particles interacting through a monotonic repulsive potential if their average separation is significantly larger than the range of their negative mean forces potential. However, for anisotropic charged disks, the repulsive pair potential varies with their

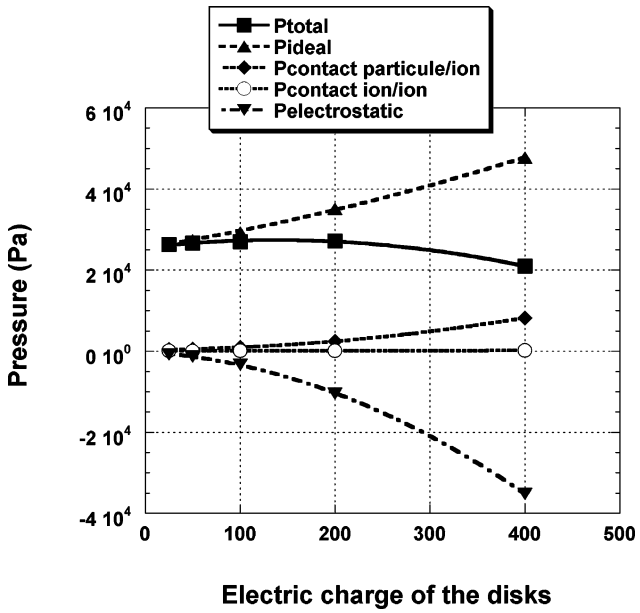

Figure 9. Variation of the total pressure of the dispersion with its various electrostatic, ideal, and contact contributions. The size of the symbols corresponds to the numerical uncertainties.

relative orientation.[22,40] As a consequence, previous Monte Carlo simulations of the organization of charged disks interacting through a site-to-site Yukawa potential[50] also exhibit a significant enhancement of the RDF in the same ranges of disk concentration (1% vol/vol) and Debye screening length (30 Å) (see Figure 4a in ref 50). Furthermore, a negative electrostatic contribution to the pair potential describing the effective interaction between charged colloids neutralized by monovalent counterions can only be interpreted on the basis of many-body effects. While such an effect has already been detected between three charged spheres[25,26] or three charged parallel cylinders[27] in the absence of salt, its occurrence is not expected to occur significantly in the presence of a large amount of salt.[51]

The only possibility to settle this question is to evaluate the swelling pressure of the dispersion and to detect a significant decrease of the ideal contribution from the corresponding disks, under the condition of the dilute regime, resulting from a negative second virial coefficient.[37] For that purpose, the total pressure is evaluated by calculating the inner virial[37] of the dispersion (see IIB above). The results displayed in Figure 9 fully agree with the details of the energetic contribution (see Figure 5) since the net electrostatic contribution to the total pressure of the dispersion of the charged disks is attractive and increases as a function of the net electric charge of disks. Repulsive contributions are dominated by the ideal contribution which is at least five times larger than the ion/disk contact repulsion while the ion/ion contact repulsion is almost negligible. As a consequence of that delicate balance between these antagonistic contributions, the total pressure within the dispersion is almost independent of the net electric charge of the disks except for a small decrease detected at the largest electric charge. As a consequence of the large amount of salt in the reservoir ($c_{salt}^{reservoir} = 5 \times 10^{-3}$ M), the swelling pressure of the dispersion

$$\Pi = P - 2kTc_{salt}^{reservoir}\gamma(I) = P - (2.3 \times 10^4 \text{ Pa}) \quad (9)$$

becomes negative. In eq 9, the salt activity coefficient ($\gamma(I) = 0.926$) is taken from previous GCMC simulations.[5]

This result suggests the possible existence of an instability of the dispersion resulting from the electrostatic coupling which may be responsible for the flocculation of the Laponite dispersion in the presence of salt.[41−42] To settle this question, it is necessary to perform the same simulations for charged disks bearing the electric charge of the Laponite clay (i.e., twice the largest value considered here). One must, however, remain very careful in interpreting such results because the measured swelling pressure of the dispersion (∼500 Pa)[41] is 2 orders of magnitude smaller than the total pressure in the dispersion and its reservoir (∼2×10^4 Pa). As a consequence, a 10% uncertainty on the evaluation of the ion/disk contact repulsion, which is of the order of magnitude of 10^4 Pa (see Figure 9), may lead to erroneous conclusions because it is larger than the measured swelling pressure. To reduce the numerical uncertainties in the derivation of the swelling pressure, further simulations must be performed at reduced salt concentration in order to enhance the range of the electrostatic coupling.[9−10] By calculating the swelling pressure at different disk densities, it is possible to extract the second virial coefficient with a better accuracy or at least determine its sign.

Another question concerns the influence of the heterogeneities of the clay size[36] and electric charge on the mechanical stability of the clay dispersion and its microsegregation.[18−19] Monte Carlo simulations of a large collection of charged anisotropic colloids should be able to elucidate that question. One may be also tempted to systematically investigate the influence of the salt concentration and the colloid density on the mechanical and structural properties of the dispersions. The validity of this hierarchical approach however imposes a strong limitation: in all cases, the Debye screening length must remain much larger than the critical distance at which the long-range Coulombic potential is replaced by its multipolar expansion.

IV. Conclusion

A hierarchical approximation of the electrostatic coupling within a large collection of charged disks was used to probe, by Monte Carlo simulations, the influence of the electrostatic coupling on the structure and the mechanical stability within colloidal dispersions of charged anisotropic nanoparticles in the presence of salt. By analyzing the influence of the gradual increase of the electric charge of the charged disks on their self-organization within the dispersion, it was possible to exhibit an attractive electrostatic contribution to the mean force potential. This result may be interpreted either by an attractive pair potential between the charged disk or by some enhancement of the radial distribution function induced by a strong repulsion between the colloids. A derivation of the second virial coefficient should be able to settle this question. Unfortunately, the results from our GCMC simulations are not significant because of the large numerical uncertainties in the derivation of the swelling pressure.

Acknowledgment. We cordially thank Drs. J. Puibasset, P. Levitz, L. Michot, and S. Bhattacharyya for helpful discussions during the progress of this work. Monte Carlo simulations were performed locally on workstations purchased thanks to grants from Région Centre (France).

References and Notes

(1) Derjaguin, B.; Landau, L. D. *Acta Physicochim. URSS* **1941**, *14*, 635.

(2) Verwey, E. J. W.; Overbeek, J. T. G. *Theory of the Stability of Lyophobic Colloids*; Elsevier: New York, 1948.

(3) Kjellander, M.; Marcelja, S.; Pashley, R. M.; Quirk, J. P. *J. Phys. Chem.* **1988**, *92*, 6489.

(4) Pellenq, R. J. M.; Caillol, J. M.; Delville, A. *J. Phys. Chem. B* **1997**, *101*, 8584.
(5) Delville, A. *J. Phys. Chem. B* **2002**, *106*, 7860.
(6) Gouy, G. *J. Phys.* **1910**, *9*, 457.
(7) Chapman, D. L. *Philos. Mag.* **1913**, *25*, 475.
(8) Langmuir, I. *J. Chem. Phys.* **1938**, *6*, 873.
(9) Israelachvili, J. N. *Intermolecular and Surface Forces*; Academic Press: London, 1985.
(10) Dubois, M.; Zemb, Th.; Belloni, L.; Delville, A.; Levitz, P.; Setton, R. *J. Chem. Phys.* **1992**, *96*, 2278.
(11) Sohm, R.; Tadros, Th. F. *J. Colloid Interface Sci.* **1989**, *132*, 62.
(12) Rand, B.; Pekenc, E.; Goodwin, J. W.; Smith, R. W. *J. Chem. Soc., Faraday Trans. 1* **1980**, *76*, 225.
(13) Forsyth, P. A.; Marcelja, S.; Mitchell, D. J.; Ninham, B. W. *Adv. Colloid Interface Sci.* **1978**, *9*, 37.
(14) Onsager, L. *Ann. N. Y. Acad. Sci.* **1949**, *51*, 627.
(15) Decruppe, J. P.; Lerouge, S.; Azzouzi, H. *Phys. Rev. E* **2005**, *71*, 011503.
(16) Van der Beek, D.; Schilling, T.; Lekkerkerker, H. N. W. *J. Chem. Phys.* **2004**, *121*, 5423.
(17) Kimura, T.; Yoshino, M. *Langmuir*, **2005**, *21*, 4805.
(18) Li, L.; Harnau, L.; Rosenfeldt, S.; Ballauff, M. *Phys. Rev. E* **2005**, *72*, 051504.
(19) Levitz, P.; Lécolier, E.; Mourchid, A.; Delville, A.; Lyonnard, S. *Europhys. Lett.* **2000**, *49*, 672.
(20) Delville, A. *J. Phys. Chem. B* **1999**, *103*, 8296.
(21) Delville, A.; Levitz, P. *J. Phys. Chem. B* **2001**, *105*, 663.
(22) Meyer, S.; Levitz, P.; Delville, A. *J. Phys. Chem. B* **2001**, *105*, 10684.
(23) Trizac, E.; Bocquet, L.; Agra, R.; Weis, J. J.; Aubouy, M. *J. Phys.: Condens. Matter* **2002**, *14*, 9339.
(24) Carley, D. D. *J. Chem. Phys.* **1967**, *46*, 3783.
(25) Löwen, H.; Allahyarov, E. *J. Phys.: Condens. Matter* **1998**, *10*, 4147.
(26) Wu, J. Z.; Bratko, D.; Blanch, H. W.; Prausnitz, J. M. *J. Chem. Phys.* **2000**, *113*, 3360.
(27) Delville, A. *Langmuir* **2003**, *19*, 7094.
(28) Kutter, S.; Hansen, J. P.; Sprik, M.; Boek, E. *J. Chem. Phys.* **2000**, *112*, 311.
(29) Harnau, L.; Costa, D.; Hansen, J. P. *Europhys. Lett.* **2001**, *53*, 729.
(30) Dijkstra, M.; Hansen, J. P.; Madden, P. A. *Phys. Rev. E* **1997**, *55*, 3044.
(31) Ding, H. Q.; Karasawa, N.; Goddard, W. A. *J. Chem. Phys.* **1992**, *97*, 4309.
(32) Meyer, S.; Levitz, P.; Delville, A. *J. Phys. Chem. B* **2001**, *105*, 9595.
(33) Frenkel, D.; Smit, B. *Understanding Molecular Simulation*; Academic Press: London, 1996.
(34) Mezei, M. *Mol. Biol.* **1980**, *40*, 901.
(35) Lachet, V.; Boutin, A.; Tavitian, B.; Fuchs, A. *Faraday Discuss.* **1997**, 106, 307.
(36) Balnois, E.; Durand-Vidal, S.; Levitz, P. *Langmuir* **2003**, *19*, 6633.
(37) Hansen, J. P.; McDonald, I. R *Theory of Simple Liquids*; Academic Press: London, 1986.
(38) Nezbeda, I. *Mol. Phys.* **1977**, *33*, 1287.
(39) Delville, A.; Porion, P.; Faugère, A. M. *J. Phys. Chem.* **2000**, *104*, 1546.
(40) Agra, R.; Trizac, E.; Bocquet L. *Eur. Phys. J. E* **2004**, *15*, 345.
(41) Eppenga, R.; Frenkel, D. *Mol. Phys.* **1984**, *52*, 1303.
(42) Mourchid, A.; Delville, A.; Lambard, J.; Lécolier, E.; Levitz, P. *Langmuir* **1995**, *11*, 1942.
(43) Mongondry, Ph.; Tassin, J. F.; Nicolaï, T. *J. Colloid Interface Sci.* **2005**, *283*, 397.
(44) Porion, P.; Al Mukhtar, M.; Meyer, S.; Faugère, A. M.; van der Maarel, J. R. C.; Delville, A. *J. Phys. Chem.* **2001**, *105*, 10505.
(45) Porion, P.; Rodts, S.; Al Mukhtar, M.; Faugère, A. M.; Delville A. *Phys. Rev. Lett.* **2001**, *87*, 208302.
(46) Porion, P.; Al Mukhtar, M.; Faugère, A. M.; Pellenq, R. J. M.; Meyer, S.; Delville A. *J. Phys. Chem.* **2003**, *107*, 4012.
(47) Porion, P.; Al Mukhtar, M.; Faugère, A. M.; Delville A. *J. Phys. Chem.* **2004**, *108*, 10825.
(48) Porion, P.; Faugère, A. M.; Delville, A. *J. Phys. Chem.* **2005**, *109*, 20145.
(49) Delville, A. *J. Phys. Chem. B* **2004**, *108*, 9984.
(50) Odriozola, G.; Romero-Bastida, M.; Guevara-Rodrigez, F. de J. *Phys. Rev. E* **2004**, *70*, 021405.
(51) Dobnikar, J.; Rzehak, R.; von Grünberg, H. H. *Europhys. Lett.* **2003**, *61*, 695.